

Constraints on the origin of the first light from SN 2014J

A. Goobar¹, M. Kromer², R. Siverd³, K. G. Stassun^{3,4}, J. Pepper^{3,5}, R. Amanullah¹,
M. Kasliwal⁶, J. Sollerman², F. Taddia²

ariel@fysik.su.se

Abstract

We study the very early lightcurve of supernova 2014J (SN 2014J) using the high-cadence broad-band imaging data obtained by the Kilodegree Extremely Little Telescope (KELT), which fortuitously observed M 82 around the time of the explosion, starting more than two months prior to detection, with up to 20 observations per night. These observations are complemented by observations in two narrow-band filters used in an H α survey of nearby galaxies by the intermediate Palomar Transient Factory (iPTF) that also captured the first days of the brightening of the SN. The evolution of the lightcurves is consistent with the expected signal from the cooling of shock heated material of large scale dimensions, $\gtrsim 1R_{\odot}$. This could be due to heated material of the progenitor, a companion star or pre-existing circumstellar environment, e.g., in the form of an accretion disk. Structure seen in the lightcurves during the first days after explosion could also originate from radioactive material in the outer parts of an exploding white dwarf, as suggested from the early detection of gamma-rays. The model degeneracy translates into a systematic uncertainty of ± 0.3 days on the estimate of the first light from SN 2014J.

Subject headings: supernovae: individual(SN 2014J)

¹The Oskar Klein Centre, Department of Physics, Stockholm University, SE 106 91 Stockholm, Sweden

²The Oskar Klein Centre, Department of Astronomy, Stockholm University, SE 106 91 Stockholm, Sweden

³Vanderbilt University, Department of Physics & Astronomy, VU Station B 1807, Nashville, TN 37235, USA

⁴Fisk University, Physics Department, 1000 17th Ave. N., Nashville, TN 37208, USA

⁵Lehigh University, Department of Physics, 413 Deming Lewis Lab, 16 Memorial Drive East Bethlehem, PA 18015, USA

⁶Observatories of the Carnegie Institution for Science, 813 Santa Barbara St, Pasadena CA 91101, USA

1. Introduction

Type Ia supernovae (SNe Ia) rank among the sharpest tools to measure the expansion history of the Universe. However, the ultimate limiting factor in their use for precision cosmology rests on our ability to control systematic uncertainties of astrophysical nature, most notably due to extinction and a possible brightness evolution over cosmic time (see Goobar & Leibundgut 2011, for a recent review). Due to its remarkably close distance, SN 2014J in M 82 ($d \sim 3.5$ Mpc) presents us with unique opportunities to study the environment and reddening of an otherwise normal SN Ia (Goobar et al. 2014; Amanullah et al. 2014; Kelly et al. 2014; Marion et al. 2014; Foley et al. 2014; Brown et al. 2014; Ashall et al. 2014), and even the impact of the intervening dust on the polarization signal (Patat et al. 2014; Kawabata et al. 2014). Moreover, its proximity allowed for the first time the direct detection of gamma-rays from the ^{56}Ni decay sequence (Churazov et al. 2014; Diehl et al. 2014) that power the optical display of SNe Ia. Contrary to expectations from most theoretical models, the detection of characteristic lines of the ^{56}Ni decay arising 20 days past explosion seems to indicate the presence of radioactive material close to the surface of the SN ejecta (Diehl et al. 2014).

Prior to this event, SN 2011fe in M 101 ($d \sim 6.4$ Mpc) was the best studied SN Ia. In particular, Nugent et al. (2011) and Bloom et al. (2012) performed studies of the early lightcurve to conclude that the explosion originated from a compact object, $R \lesssim 0.02 R_{\odot}$, i.e., the size of a white dwarf (WD), as expected from models where SNe Ia result from a thermonuclear explosion in a C/O WD (Hoyle & Fowler 1960). The validity of the tight limit has been questioned by Piro & Nakar (2014), who suggested there could be a “dark phase” of up to a few days between the explosion and the rise of the radioactively powered lightcurve. Due to the lack of well-sampled deep observations prior to discovery, a possible early burst of light cannot be safely ruled out. Further discussions on the early rise of SNe Ia have been provided by Piro (2012); Piro & Nakar (2013) and Dessart et al. (2014). From a spectroscopic analysis of SN 2011fe Mazzali et al. (2014) derived a dark phase of ~ 1 day, resulting in a limit of $R \lesssim 0.06 R_{\odot}$ for the progenitor size.

For SN 2014J, Zheng et al. (2014) reported January 14.75 UT (± 0.21 day) as the best estimate of the explosion date, based on observations from the Katzman Automatic Imaging Telescope (KAIT) at Lick Observatory and amateur data from K. Itagaki¹. They also conclude that a fire-ball model (Riess et al. 1999), where the luminosity is assumed to scale with the area of the expanding photosphere at constant temperature and expansion velocity, $L \sim t^2$, does not provide a good description to the KAIT data of SN 2014J and used instead a

¹<http://www.k-itagaki.jp/psn-m82.jpg>

broken power-law expression to derive the time of first light. Similarly, Goobar et al. (2014) showed that the early data of SN 2014J from the intermediate Palomar Transient Factory (iPTF) obtained with the 48-inch telescope (P48) in two narrow-band $H\alpha$ filters deviate from the simple t^2 law.

In this work, we investigate the possibility that the deviations from a simple t^2 rise seen in the lightcurves of SN 2014J originate from an extra source of luminosity from either shock-heating of the ejecta, interaction with circumstellar matter or a companion star; or from radioactive material in the outer parts of the exploding star. For this purpose, we use the early iPTF narrow-band data from Goobar et al. (2014) and the high-cadence observations from the Kilodegree Extremely Little Telescope (KELT) from (Siverd et al. 2014)

2. Observations

The effective filter pass-bands (i.e., including the telescope optics, CCD sensitivity and atmospheric throughput) used for the early observations of SN 2014J from iPTF (Goobar et al. 2014) and KELT (Siverd et al. 2014) are shown in Fig. 1, along with the SN 2014J classification spectrum (Cao et al. 2014) from January 22. The SN exploded around full moon, when iPTF was conducting a narrow-band survey of the Galactic plane and neighbouring galaxies with the Palomar 48-inch telescope. Thus, the first set of iPTF imaging observations were conducted with $H\alpha$ filters centred at 6564 Å and 6638 Å, respectively. Also shown in Fig. 1 is the full (currently) available KELT lightcurve, starting about two months prior to explosion and reaching to about day +140 after lightcurve maximum.

KELT is primarily an exoplanet transit survey (Pepper et al. 2007), using a small aperture telescope (42 mm) with a very wide FoV, $26^\circ \times 26^\circ$ and a broad transmission function, $X(\lambda)$, cutting around 4600 Å on the blue side and reaching into the near-IR, $\lambda \sim 1\mu\text{m}$. The effective wavelength of the KELT pass-band (filter plus CCD response) is $\lambda_{\text{eff}} \approx 691$ nm. KELT has a very coarse pixel scale, $\sim 23''$, which makes accurate SN photometry challenging (Siverd et al. 2014). The KELT-North telescope obtained a total of 1869 individual exposures of SN 2014J that meet the quality control cuts. These exposures span 249 nights starting on 08 October 2013 and ending on 14 June 2014.

Because the KELT-North telescope uses a German Equatorial mount, observations taken before and after the local median crossing involve a 180-degree flip of the FOV, which we designate West and East exposures. In order to avoid systematics in the flux scale between the West and East exposures, we restrict our analysis below to the West exposures. Therefore the final KELT lightcurve includes 889 individual exposures spanning 10 November 2013 to

14 June 2014 (Julian Dates 2456607.03 to 2456822.69). East and West are defined according to the sky position of the target, not by the orientation of the mount. In other words, the East exposures are acquired earlier in the night. There is in general an offset (and a scaling) difference between the East and West photometry. Consequently, the East and West data are reduced independently and have a different flux scale. We found empirically that the West data have a better behaved PSF and smaller sky contamination, and therefore have overall better precision. Here we have opted to work with just the West orientation because of the better precision but most importantly to avoid systematics that could not be removed if attempting to also include the East data.

On nights with good weather where at least one measurement was obtained, the number of measurements per night varies from 1 to 20. Note that the KELT observing procedure employs a Moon avoidance strategy, which leads to increased cadence on fields that are more than 60 degrees away from the Moon. Fortunately, this Moon avoidance led to increased cadence on the M 82 field around the time of the explosion of SN 2014J. Flux measurements from the individual KELT-North frames are extracted using the difference-imaging aperture photometry pipeline described in Siverd et al. (2014), which is a modified version of the standard KELT pipeline (see Siverd et al. 2012). Briefly, the standard KELT pipeline was modified to deal with the non-optimal placement of M 82 near a corner of the KELT FOV, leading to poor extraction with the standard pipeline. Instead, in the modified pipeline, the photometry extraction was manually forced to a custom cutout region centered on M 82. Each photometric measurement is a differential measurement relative to a template image by means of image subtraction. The template image is the median of 130 images obtained during the month prior to the explosion.

Typically, KELT achieves a photometric precision of 1% or better on point sources brighter than $V \approx 10$. In the case of SN 2014J, the KELT lightcurve achieved a photometric precision of 1.5% on average at peak brightness, and 3% on average at half peak brightness.

Photometry of the iPTF images was carried out with the method used in Amanullah et al. (2008). PSF photometry of the SN fluxes of all epochs together with the background host-galaxy light was fitted simultaneously. The degeneracy between the host and the SN was broken by fixing the SN flux to zero for all epochs obtained in 2013. Lightcurves were also built of 240 stars in the fields, which were used for calibration as well as for deriving systematic uncertainties between the epochs. The former was carried out by matching the field star photometry to SDSS DR10 r' and i' magnitudes. The uncertainty for individual epochs was found to be 0.03 mag and the uncertainty of the calibration is good to 0.07 mag. The photometry for the early rise used in this analysis is summarized in Table 1.

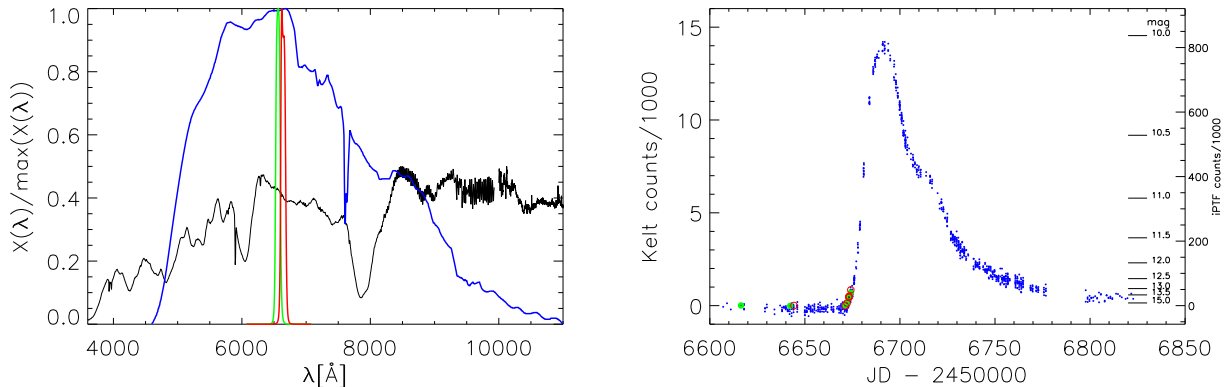


Fig. 1.— *Left*: System transmission functions $X(\lambda)$ for the KELT (broad-band; blue) and iPTF (narrow filters; green/red) used for the early observations of SN 2014J. Also shown in black is the earliest spectrum available, F_λ , from Cao et al. (2014), about 7 days after the derived explosion date. *Right*: The KELT (blue) and iPTF (red, green) light curve points. KELT covers epochs from about two months prior to explosion to day 140 after peak. Also shown are the natural Vega magnitudes for the calibrated fluxes.

3. Early lightcurves of SNe Ia

Observationally, the early lightcurve shapes for SNe Ia follow, to a good approximation, a power-law behaviour. For SN 2011fe, hitherto the object with the best-covered early-time lightcurve, Nugent et al. (2011) found $L \propto t^\beta$, with $\beta = 2.01 \pm 0.01$. Studies of stacked lightcurves of a nearby SN Ia sample from the LOSS survey (Ganeshalingam et al. 2011), typically not quite as sensitive to the very early phases, $t \lesssim 1$ day, found $\beta = 2.20^{+0.27}_{-0.19}$. Similarly, a lightcurve analysis of SDSS-II supernovae at cosmological distances by Hayden et al. (2010) found $\beta = 1.8^{+0.23}_{-0.18}$, compatible with a similar study of SNLS SNe Ia, $\beta = 1.8 \pm 0.2$, (Conley et al. 2006). Recently, Firth et al. (2014) studied a sample of 18 SNe Ia from the Palomar Transient Factory (PTF) and the La Silla-QUEST variability survey (LSQ) and found a mean value of $\beta = 2.44 \pm 0.13$.

Nugent et al. (2011) and Piro (2012) have shown that such a power-law behaviour can in principle result from radioactive heating of the supernova ejecta. However, the exact shape of the rise will depend on the particular gradients in velocity, density and chemical composition within the ejecta (Piro 2012). In particular, estimating the SN explosion epoch by fitting a power law to the early-time lightcurve might be misleading (Piro & Nakar 2014). Explosion models that can explain the observed properties of normal SNe Ia like delayed detonations in Chandrasekhar-mass WDs (e.g. Kasen et al. 2009; Sim et al. 2013; Dessart et al. 2014)

or violent WD-WD mergers (Pakmor et al. 2012), predict that most ^{56}Ni should be buried in the central part of the ejecta and not reach to the outermost layers. As a consequence, it will take some time for the radioactive energy to diffuse to the surface of the SN ejecta and a dark phase might occur between the onset of explosion and the time of first light (Piro & Nakar 2013, 2014).

3.1. Cooling of shock-heated SN ejecta

While the SN shock wave propagates through the progenitor star, it deposits energy all over the ejecta. Due to efficient adiabatic cooling this shock deposited energy becomes negligible (with respect to radioactive heating) at ~ 1 day after explosion for a WD progenitor. At very early times, however, radiative diffusion from shock-heated outer layers of the SN ejecta may contribute to the emergent luminosity. In the past, several groups have investigated the cooling of shock heated SN ejecta with analytical frameworks, e.g. Chevalier (1992); Piro et al. (2010); Kasen (2010); Nakar & Sari (2010); Rabinak & Waxman (2011). Assuming spherically symmetric, radiation dominated, homologously expanding SN ejecta with constant opacity, the different approaches vary in their treatment of radiative diffusion and opacity and their assumption of the initial density and pressure profiles. However, recent work has shown that the different approaches agree within a factor of ~ 2 (Rabinak & Waxman 2011).

Here, we follow the approach in Nugent et al. (2011) and Bloom et al. (2012) who use the model of Rabinak & Waxman (2011) to calculate the early-time luminosity (L^E) and temperature (T^E) from shock heated ejecta:

$$\begin{aligned} L^E(t) &= 1.2 \cdot 10^{40} R_{10} (E_{51})^{0.85} (M_c)^{-0.69} (\kappa_{0.2})^{-0.85} (f_p)^{-0.16} (t_d)^{-0.31} \text{ erg s}^{-1} \\ T_{\text{eff}}^E(t) &= 4.1 \cdot 10^3 (R_{10})^{0.25} (E_{51})^{0.016} (M_c)^{0.03} (\kappa_{0.2})^{0.27} (f_p)^{-0.022} (t_d)^{-0.47} \text{ K}, \end{aligned} \quad (1)$$

where R_{10} is the progenitor radius in units of 10^{10} cm, E_{51} the explosion energy in units of 10^{51} erg, M_c the progenitor mass in units of the Chandrasekhar mass ($1.38M_\odot$), $\kappa_{0.2}$ the opacity in units of $0.2 \text{ cm}^2\text{g}^{-1}$, f_p a form factor that depends on the density profile of the progenitor star and t_d the time since explosion in days. In the following we adopt $E_{51} = 1$, $M_c = 1$, $\kappa_{0.2} = 1$ and $f_p = 0.05$.

3.2. Cooling of a shock-heated companion star

Similar to the situation discussed in the previous section, the SN shock wave will heat the surface layers of a surviving companion star, if present. This shock deposited energy

may then contribute to the early-time luminosity of the SN. This scenario was investigated by Kasen (2010). From a multi-dimensional radiative transfer simulation, Kasen showed that the emerging flux is strongly angle dependent. For favourable viewing angles, i.e. those lying within the hole that is carved out of the SN ejecta by interaction between the ejecta and the companion star, shock heating of the companion star leads to a significant flux excess at early times compared to pure radioactive heating. Hydrodynamical simulations of interactions between the SN ejecta and the companion star show that the half opening angle of such ejecta holes is $\sim 30 - 40$ degrees (e.g. Marietta et al. 2000; Pakmor et al. 2008). In contrast, from the opposite direction the optically thick ejecta are obscuring the companion and no effect of the shock heating is present, as shown in Fig. 2 of Kasen (2010).

Kasen (2010) provides an analytic fit formula for the evolution of the early-time bolometric luminosity and temperature, L^C and T^C :

$$\begin{aligned} L^C(t) &= 10^{43} a_{13} (M_c)^{1/4} (v_9)^{7/4} (\kappa_e)^{-3/4} (t_d)^{-1/2} \text{ erg s}^{-1} \\ T_{\text{eff}}^C(t) &= 2.5 \cdot 10^4 (a_{13})^{1/4} (\kappa_e)^{-35/36} (t_d)^{-37/72} \text{ K.} \end{aligned} \quad (2)$$

Here, a_{13} is the separation distance between the SN progenitor and its companion in units of 10^{13} cm, M_c the progenitor mass in units of the Chandrasekhar mass, v_9 the expansion velocity of the SN ejecta in units of 10^9 cm s^{-1} , κ_e the electron scattering opacity in units of $0.2 \text{ cm}^2 \text{ g}^{-1}$ and t_d the time since explosion in days. In the following we adopt $M_c = 1$, $\kappa_e = 1$ and $v_9 = 1$. Assuming that the companion fills its Roche lobe, its radius can be constrained to be $\lesssim 0.5 a_{13}$.

4. Analysis of the early lightcurves of SN 2014J

Zheng et al. (2014) pointed out that the early broad-band lightcurve of SN 2014J does not follow a unique power law. Instead a broken power-law expression was used to fit the data for the purpose of deriving the explosion date. Apart from SN 2014J, there is today only one other SN known that shows such a behaviour (SN 2013dy, Zheng et al. 2013). For the bulk of observed SNe Ia the lightcurve rise is in good agreement with a single power law (Conley et al. 2006; Hayden et al. 2010; Ganeshalingam et al. 2011).

In what follows, we will try to reconcile the deviant behaviour of SN 2014J as being a combination of (at least) two effects: radioactive heating from the inner ejecta and some extra component, e.g. from shock-heating of the ejecta or a companion; or surface radioactivity, described in Section 4.4.

4.1. The fitting procedure

Given the empirical evidence for a power-law behaviour for the radioactive early lightcurve of a large body of SNe Ia, we assume that the SN flux through a system transmission function $X(\lambda)$ (see Fig. 1) can be described by the sum of two components, including one of the terms in Eqns (1) or (2) and a power-law:

$$\mathcal{F}_X(t) = \begin{cases} C_X(t - t_0)^\beta + \int \frac{\mathcal{L}^\delta(\lambda, t - t_0)}{4d^2} X(\lambda) 10^{\left(-\frac{A_\lambda}{2.5}\right)} d\lambda & t \geq t_0 \\ 0 & t < t_0, \end{cases} \quad (3)$$

where δ is an index specifying the source of luminosity (e.g., heating of ejecta or companion star) and A_λ corresponds to the adopted extinction law, where for SN 2014J we base our extinction corrections on the parameters in Amanullah et al. (2014), and $\mathcal{L}^\delta(\lambda, t)$ is the wavelength dependent luminosity:

$$\mathcal{L}^\delta(\lambda, t) = L^\delta(t) \cdot \frac{B_\lambda(T_{\text{eff}}^\delta(t))}{\sigma_{\text{SB}} [T_{\text{eff}}^\delta(t)]^4}, \quad (4)$$

where we have assumed a black-body spectral energy distribution (SED) and used the Stefan-Boltzmann law.

Next, we use the above expressions to fit the measured SN lightcurves for the first four days after the explosion, along with pre-explosion data to derive the explosion time, t_0 and the physical parameters of the extra source of energy. For the case of shock-heated ejecta, we fit the radius of the progenitor star. When investigating the interaction with the companion, the parameter of interest is the radius of the companion star, assuming Roche-lobe filling.

It should be noted that the adopted phenomenological description in Eq. (3) cannot be exact since, at any given time, the two contributions will not be completely independent. E.g., the same parts of the ejecta may contribute due to shock heating and radioactive heating. However, in the limit of $t \rightarrow 0$ the shock heating will dominate, while for $t \rightarrow \infty$ radioactive heating is the main source of energy for the optical lightcurves. Similarly, the fitted power-law component could absorb some of the contributions of the extra source of power.

We choose to fit the data in flux space (not magnitudes) to minimise potential bias effects. This is important since for $t < t_0$ positive as well as negative fluctuations should be treated equally. Furthermore, the (mainly) Poisson noise is simple to characterise in linear flux space.

4.2. Verification of the method using observations of SN 2011fe

We first verify our method by revisiting the results on SN 2011fe based on the g -band magnitudes reported by Nugent et al. (2011), also adopting their assumed distance to M 101 of 6.4 Mpc and negligible extinction A_λ . For the epochs with non-detections, we set the flux to zero and assign the (symmetric) 1σ error bar from the reported upper limits in Table 1 of Nugent et al. (2011). The fit results are shown in the two top panels of Fig. 2, where one can see that our results are in good agreement with Nugent et al. (2011) and Bloom et al. (2012). In particular, we find that a combination of a power-law model ($\beta = 2$) with shock heating of a compact progenitor of radius $R = 0.02R_\odot$ provides an excellent fit, as shown in Fig. 2(a). For the interaction with the companion, as specified by the model of Kasen (2010) described in Section 3.2, we find in Fig. 2(b) that a companion star of size $R \lesssim 0.25R_\odot$ provides a good fit to the observed g -band lightcurve, i.e., slightly less constraining than the limits found by Bloom et al. (2012), $R < 0.1R_\odot$. The small discrepancy is likely connected to the different analysis approaches, i.e., the use of flux space and two components in the fit.

4.3. Fits of the combined iPTF/KELT data of SN 2014J

For the analysis of the early imaging data of SN 2014J we use the same methodology as for SN 2011fe in Sec. 4.2. For the system transmissions of iPTF and KELT we use the functions $X(\lambda)$ shown in Fig. 1. Furthermore, we adopt the distance to M 82 from Dalcanton et al. (2009), $d = 3.5$ Mpc, and the host galaxy reddening of SN 2014J derived by Amanullah et al. (2014), where we opted to use their parameter solution for the Galactic type extinction model of Fitzpatrick (1999), $R_V = 1.4$, $E(B - V)_{\text{host}} = 1.37$ mag. Exchanging to the multiple scattering model of Goobar (2008), found to give a slightly better fit to the full multi-wavelength lightcurve data from UV to the near-IR in Amanullah et al. (2014) and Foley et al. (2014), does not have a major impact on the outcome of the fits. We also include Milky-Way reddening, $R_V = 3.1$, $E(B - V)_{MW} = 0.06$ mag. We have assumed the dust causing the reddening is sufficiently far from the site of the SN that there is no significant change in the reddening properties over time. The results of the fits for $\beta \equiv 2$ are shown in the two bottom panels of Fig. 2.

The lightcurves of the three filters are fitted simultaneously. The number of degrees of freedom and the χ^2 for the best fit are also indicated in the figure. Clearly, the fits are statistically very sound and no systematic deviations are found for any of the data-sets.

Since there is an arbitrary flux offset between the template image and the subsequent science images, this is accounted for in the lightcurve fitting through inclusion of a constant

offset term. Note that the offset is in fact very small, comparable to the per-night binned photometric precision (i.e., smaller than the per-point photometric precision) and does not affect the results.

Fixing $\beta \equiv 2$, as observed in other SNe Ia, we find that for the scenario where the powering of the early rise of the lightcurve is a combination of a power-law and shock heating of the ejecta, the radius of the progenitor does *not* match that of a compact object for SN 2014J (at 90 % confidence level), unlike the case for SN 2011fe. Instead, a radius in excess of the size of the Sun is required. For the assumptions made, we find a best fit for $R = 1.7R_{\odot}$. Levanon et al. (2014) argue that such large radii could be expected for WD mergers if an explosion does not occur on the dynamical time scale of the merger, as in the violent merger model (Pakmor et al. 2012), but on the longer viscous or thermal time scales of the merger remnant. In this case, angular momentum conservation leads to the formation of an accretion disc or extended envelope around the primary WD (Schwab et al. 2012) that extends to several solar radii. Whether such a configuration was present in the case of SN 2014J cannot be definitely assessed from our simple modeling. It is however interesting to note that Diehl et al. (2014) speculate about the formation of a He accretion belt to explain their detection of narrow gamma-ray lines from ^{56}Ni decay around maximum light. Detailed explosion models will be required to address this question.

When attributing the “bump” in the early lightcurve to heating of a companion star, we find that for the most optimal viewing angle (see Fig. 2 in Kasen 2010) a companion of radius $4R_{\odot}$ is required. For less favoured viewing angles, much larger companion stars would be needed to fit the observations. We also find that, if this lightcurve modeling is assumed, the explosion occurred 7 hours (0.29 days) later than using the fit based on a broken power-law lightcurve in Zheng et al. (2014). For the case of heated ejecta, our fits suggest that the explosion took place 5 hours later than the best fit value of Zheng et al. (2014).

We note that the adopted formalism in Eq. 3 implies a negligible dark phase, since the power-law component as well as the extra heating start at the same time, t_0 . Although we could (in principle) add an extra free parameter in the fitting procedure to account for a time offset between the two sources of light, the excellent goodness of fit in our results does not motivate adding more degrees of freedom. We have also investigated the effect of combining our data-set with the limits from Zheng et al. (2014) and find that this conclusion remains unchanged.

We note that it is still possible to get a formally acceptable fit for a compact progenitor and/or a small companion but only by invoking a very slow time dependence, $\beta = 1.2 - 1.3$, as shown in Fig. 3. According to Piro & Nakar (2013) such a shallow rise is possible if direct heating from ^{56}Ni is dominating the luminosity indicating radioactive material right at the

surface of the SN ejecta. This is also required to explain the detection of gamma-rays from ^{56}Ni decay as reported by Diehl et al. (2014). The explosion time is slightly perturbed, in the most extreme case by 6 hours (earlier) than in Zheng et al. (2014).

4.4. Surface radioactivity

In the following we explore the possibility that radioactive material was deposited close to the surface of the SN ejecta in more detail. Surface radioactivity is actually predicted by various explosion models, e.g. turbulent deflagrations that lead to completely mixed explosion ejecta (e.g. Gamezo et al. 2003; Fink et al. 2014) or double detonations in sub-Chandrasekhar-mass WDs where an initial detonation in an accreted helium layer can lead to radioactive isotopes close to the surface of the ejecta (e.g. Kromer et al. 2010; Woosley & Kasen 2011). How this material affects the early lightcurves in detail, depends quite sensitively on its distribution and which isotopes are produced.

Piro & Nakar (2013) presented a simplified analytical model to derive constraints on the ^{56}Ni distribution from the early bolometric lightcurve. Assuming that the radioactively powered early lightcurves scale with the amount of ^{56}Ni (M_{56}) that has been exposed at time t , the luminosity due to direct heating by ^{56}Ni is $L^{\text{rad}}(t) \approx M_{56}(t) \cdot \epsilon(t)$, with:

$$\epsilon(t) = \epsilon_{\text{Ni}} e^{-t/t_{\text{Ni}}} + \epsilon_{\text{Co}} (e^{-t/t_{\text{Co}}} - e^{-t/t_{\text{Ni}}}), \quad (5)$$

where $\epsilon_{\text{Ni,Co}}$ and $t_{\text{Ni,Co}}$ correspond to the specific heating and decay time of ^{56}Ni and ^{56}Co , respectively.

For a steep gradient of radioactive material towards the inner parts of the exploding star, the deposition of gamma-rays could be dominated by deeper layers, with a fraction of photons escaping faster than the average diffusion time. Piro & Nakar (2013) call this a “diffusive tail” (schematically shown in their Fig. 2) and derive the expected contribution to the bolometric lightcurve:

$$L^{\text{tail}}(t_0 \leq t < t') = L^{\text{rad}}(t') \frac{\epsilon(t - t_0)}{\epsilon(t' - t_0)} \frac{\text{erfc}((t' - t_0)/\sqrt{2}(t - t_0))}{\text{erfc}(1/\sqrt{2})}, \quad (6)$$

where ‘erfc’ is the complementary error function. Next, we analyze the early lightcurve data of SN 2014J through fits of the theoretical models described above making the crude assumption that the narrow and broad-band iPTF and KELT fluxes are good proxies for the bolometric luminosity, i.e., $L_{\text{bol}}(t) \propto L_X(t)$, where X correspond to the filter data available. Following a similar approach than in Sections 3.1 and 3.2, we consider the observed fluxes

to be the sum of two components:

$$\mathcal{F}_X(t) = C_X^1(t - t_0)^\beta + C_X^2 L^{\text{tail}}(t, t_0, t'). \quad (7)$$

Here we should clarify that this treatment differs from Piro & Nakar (2013), since their model aims at explaining the full lightcurve evolution, without the additional power-law term. Our treatment is empirically motivated by the good χ^2 of the fit, as shown in Fig. 4, which can be directly compared to the fits involving shock-heated material.

From the fitted luminosity, $L^{\text{tail}}(t' - t_0) = 6 \cdot 10^{-3} L_{\text{bol}}^{\text{peak}}$, and the assumption that the bolometric peak brightness is as for SN 2011fe, $L_{\text{bol}}^{\text{peak}} = 1.2 \cdot 10^{43} \text{ erg s}^{-1}$ (Pereira et al. 2013), we can estimate the amount of “shallow” ($\sim 0.1 M_\odot$ below surface) ^{56}Ni needed to power the lightcurve about 1 day after explosion, $M_{56} \approx 1.1 \cdot 10^{-3} M_\odot$, corresponding to a mixing mass fraction $X_{56} \approx 1.4 \cdot 10^{-2}$ when inserted in Eqn. 8 of Piro & Nakar (2013). We note that this falls short to match the amount of surface ^{56}Ni invoked by Diehl et al. (2014) in their modelling of the detection of gamma-rays from SN 2014J. Given the possible degeneracy in our treatment, where the power-law component may absorb some of the contribution from radioactive surface material, our estimate may be regarded as a lower limit.

5. Conclusions

We have analysed the early phase of the optical lightcurve following the explosion of SN 2014J in M 82. The high-cadence KELT data, with up to twenty visits per night, starting two months prior to the first detected light was used along with two sets of narrow-band data from iPTF. The observations are suitable for studies of the first few days following the explosion. This data-set is unique among published SN lightcurves and can be compared to the previous nearest “normal” SN Ia in modern time, SN 2011fe.

Unlike the case for SN 2011fe, a t^2 -model together with cooling from a compact progenitor does not provide the best match to the observations. Instead, we find that the required size scale of the heated material, either in the ejecta or a companion, is about a solar radius or larger. As the possibility of having a single degenerate model with a large companion has been ruled out by e.g., searches in pre-explosion HST images (Goobar et al. 2014; Kelly et al. 2014); non-detections at x-ray (Margutti et al. 2014) and radio wavelengths (Pérez-Torres et al. 2014), other explanations to our findings are needed. Following Levanon et al. (2014), WD mergers could be one possibility. If ignited on a viscous timescale rather than a dynamical time scale, an extended CSM will form around the primary WD. Shock heating of this material could be consistent with the observed early lightcurve of SN 2014J. Another possibility indicated by the shallow lightcurve rise could be that surface

radioactivity contributes to the early lightcurve evolution. This was also invoked to explain the early gamma-ray signal from ^{56}Ni decay observed in SN 2014J by (Diehl et al. 2014), albeit in larger quantities than was derived from our analysis of the optical lightcurve rise. Based on the available data, although with exquisite time sampling early on, the degeneracies between the various explanations cannot be resolved, due to insufficient signal-to-noise and color information. The model degeneracy translates into a systematic uncertainty of ± 0.3 days on the estimate of the first light from SN 2014J.

We note that new well-sampled lightcurves are to be expected soon from the ongoing KEPLER extragalactic survey². As these will be carried on in an orchestrated fashion with surveys like iPTF and KAIT, we can expect future discoveries to have a richer spectroscopic and imaging coverage early on, e.g., in the UV from Swift and HST. Methods to distinguish between the various potential sources of luminosity in the early rise of Type Ia SN lightcurves, including temperatures and line velocities have been proposed by Piro & Nakar (2014). We also note that similar attempts have been made to study the rise times of Ib/c SNe in Taddia et al. (2014). Thus, the prospects of progress in this area are good.

AG and RA acknowledge support from the Swedish Research Council and the Swedish Space Board.

REFERENCES

- Amanullah, R., Stanishev, V., Goobar, A., et al. 2008, *A&A*, 486, 375
- Amanullah, R., Goobar, A., Johansson, J., et al. 2014, *ApJ*, 788, L21
- Ashall, C., Mazzali, P., Bersier, D., et al. 2014, *ArXiv e-prints*, arXiv:1409.7066
- Bloom, J. S., Kasen, D., Shen, K. J., et al. 2012, *ApJ*, 744, L17
- Brown, P. J., Smitka, M. T., Wang, L., et al. 2014, *ArXiv e-prints*, arXiv:1408.2381
- Cao, Y., Kasliwal, M. M., & McKay, A. 2014, *The Astronomer’s Telegram*, 5786, 1
- Chevalier, R. A. 1992, *ApJ*, 394, 599
- Churazov, E., Sunyaev, R., Isern, J., et al. 2014, *Nature*, 512, 406

²http://www.astro.umd.edu/~olling/KEGS_K2.htm

H_{α}^{656} Zero-point = 24.77		
UT Jan 2014	flux	mag
14.18	-839.03 ± 952.38	
15.18	6933.76 ± 653.08	15.17 ± 0.08
16.17	23600.63 ± 631.02	13.84 ± 0.02
16.25	25762.67 ± 654.94	13.74 ± 0.02
17.17	40287.14 ± 566.79	13.26 ± 0.01
H_{α}^{663} Zero-point = 24.83		
UT Jan 2014	flux	mag
14.17	131.28 ± 970.02	
15.18	7834.99 ± 600.26	15.09 ± 0.07
16.17	25596.23 ± 694.16	13.81 ± 0.02
16.17	28185.31 ± 444.92	13.70 ± 0.01
16.22	28485.04 ± 830.09	13.69 ± 0.03
16.22	26398.80 ± 792.00	13.78 ± 0.03
17.16	48755.88 ± 713.46	13.11 ± 0.01
KELT Zero-point = 20.41		
UT Jan 2014	flux	mag
11.42	-241.71 ± 67.48	
11.52	-24.08 ± 80.86	
12.41	-70.10 ± 79.43	
12.51	-140.29 ± 89.18	
13.40	-177.58 ± 79.28	
13.52	-139.61 ± 76.93	
14.40	-73.86 ± 75.38	
14.51	-162.87 ± 75.99	
15.40	156.33 ± 79.95	14.92 ± 0.44
15.51	161.54 ± 89.63	14.89 ± 0.48
16.40	406.09 ± 82.23	13.89 ± 0.18
16.50	622.89 ± 98.03	13.42 ± 0.14
17.40	725.65 ± 68.95	13.25 ± 0.08
17.50	600.53 ± 76.19	13.46 ± 0.11
18.39	1316.60 ± 66.64	12.61 ± 0.04
18.51	1428.99 ± 77.22	12.52 ± 0.05

Table 1: Data used in this analysis. For KELT, only binned data is tabulated. The full data-set is presented in Siverd et al. (2014)

- Conley, A., Howell, D. A., Howes, A., et al. 2006, *AJ*, 132, 1707
- Dalcanton, J. J., Williams, B. F., Seth, A. C., et al. 2009, *ApJS*, 183, 67
- Dessart, L., Blondin, S., Hillier, D. J., & Khokhlov, A. 2014, *MNRAS*, 441, 532
- Diehl, R., Siebert, T., Hillebrandt, W., et al. 2014, *ArXiv e-prints*, arXiv:1407.3061
- Fink, M., Kromer, M., Seitenzahl, I. R., et al. 2014, *MNRAS*, 438, 1762
- Firth, R. E., Sullivan, M., Gal-Yam, A., et al. 2014, *ArXiv e-prints*, arXiv:1411.1064
- Fitzpatrick, E. L. 1999, *PASP*, 111, 63
- Foley, R. J., Fox, O. D., McCully, C., et al. 2014, *MNRAS*, 443, 2887
- Gamezo, V. N., Khokhlov, A. M., Oran, E. S., Chtchelkanova, A. Y., & Rosenberg, R. O. 2003, *Science*, 299, 77
- Ganeshalingam, M., Li, W., & Filippenko, A. V. 2011, *MNRAS*, 416, 2607
- Goobar, A. 2008, *ApJ*, 686, L103
- Goobar, A., & Leibundgut, B. 2011, *Annual Review of Nuclear and Particle Science*, 61, 251
- Goobar, A., Johansson, J., Amanullah, R., et al. 2014, *ApJ*, 784, L12
- Hayden, B. T., Garnavich, P. M., Kessler, R., et al. 2010, *ApJ*, 712, 350
- Hoyle, F., & Fowler, W. A. 1960, *ApJ*, 132, 565
- Kasen, D. 2010, *ApJ*, 708, 1025
- Kasen, D., Röpke, F. K., & Woosley, S. E. 2009, *Nature*, 460, 869
- Kawabata, K. S., Akitaya, H., Yamanaka, M., et al. 2014, *ArXiv e-prints*, arXiv:1407.0452
- Kelly, P. L., Fox, O. D., Filippenko, A. V., et al. 2014, *ApJ*, 790, 3
- Kromer, M., Sim, S. A., Fink, M., et al. 2010, *ApJ*, 719, 1067
- Levanon, N., Soker, N., & García-Berro, E. 2014, *ArXiv e-prints*, arXiv:1408.1375
- Margutti, R., Parrent, J., Kamble, A., et al. 2014, *ApJ*, 790, 52
- Marietta, E., Burrows, A., & Fryxell, B. 2000, *ApJS*, 128, 615

- Marion, G. H., Sand, D. J., Hsiao, E. Y., et al. 2014, ArXiv e-prints, arXiv:1405.3970
- Mazzali, P. A., Sullivan, M., Hachinger, S., et al. 2014, MNRAS, 439, 1959
- Nakar, E., & Sari, R. 2010, ApJ, 725, 904
- Nugent, P. E., Sullivan, M., Cenko, S. B., et al. 2011, Nature, 480, 344
- Pakmor, R., Kromer, M., Taubenberger, S., et al. 2012, ApJ, 747, L10
- Pakmor, R., Röpke, F. K., Weiss, A., & Hillebrandt, W. 2008, A&A, 489, 943
- Patat, F., Taubenberger, S., Cox, N. L. J., et al. 2014, ArXiv e-prints, arXiv:1407.0136
- Pepper, J., Pogge, R. W., DePoy, D. L., et al. 2007, PASP, 119, 923
- Pereira, R., Thomas, R. C., Aldering, G., et al. 2013, A&A, 554, A27
- Pérez-Torres, M. A., Lundqvist, P., Beswick, R. J., et al. 2014, ApJ, 792, 38
- Piro, A. L. 2012, ApJ, 759, 83
- Piro, A. L., Chang, P., & Weinberg, N. N. 2010, ApJ, 708, 598
- Piro, A. L., & Nakar, E. 2013, ApJ, 769, 67
- . 2014, ApJ, 784, 85
- Rabinak, I., & Waxman, E. 2011, ApJ, 728, 63
- Riess, A. G., Filippenko, A. V., Li, W., et al. 1999, AJ, 118, 2675
- Schwab, J., Shen, K. J., Quataert, E., Dan, M., & Rosswog, S. 2012, MNRAS, 427, 190
- Sim, S. A., Seitzzahl, I. R., Kromer, M., et al. 2013, MNRAS, 436, 333
- Siverd, R. J., Beatty, T. G., Pepper, J., et al. 2012, ApJ, 761, 123
- Siverd, R. J., Goobar, A., Stassun, K. G. & Pepper, J. 2014, ArXiv e-prints, arXiv:1411.4150
- Taddia, F., Sollerman, J., Leloudas, G., et al. 2014, ArXiv e-prints, arXiv:1408.4084
- Woosley, S. E., & Kasen, D. 2011, ApJ, 734, 38
- Zheng, W., Silverman, J. M., Filippenko, A. V., et al. 2013, ApJ, 778, L15
- Zheng, W., Shivvers, I., Filippenko, A. V., et al. 2014, ApJ, 783, L24

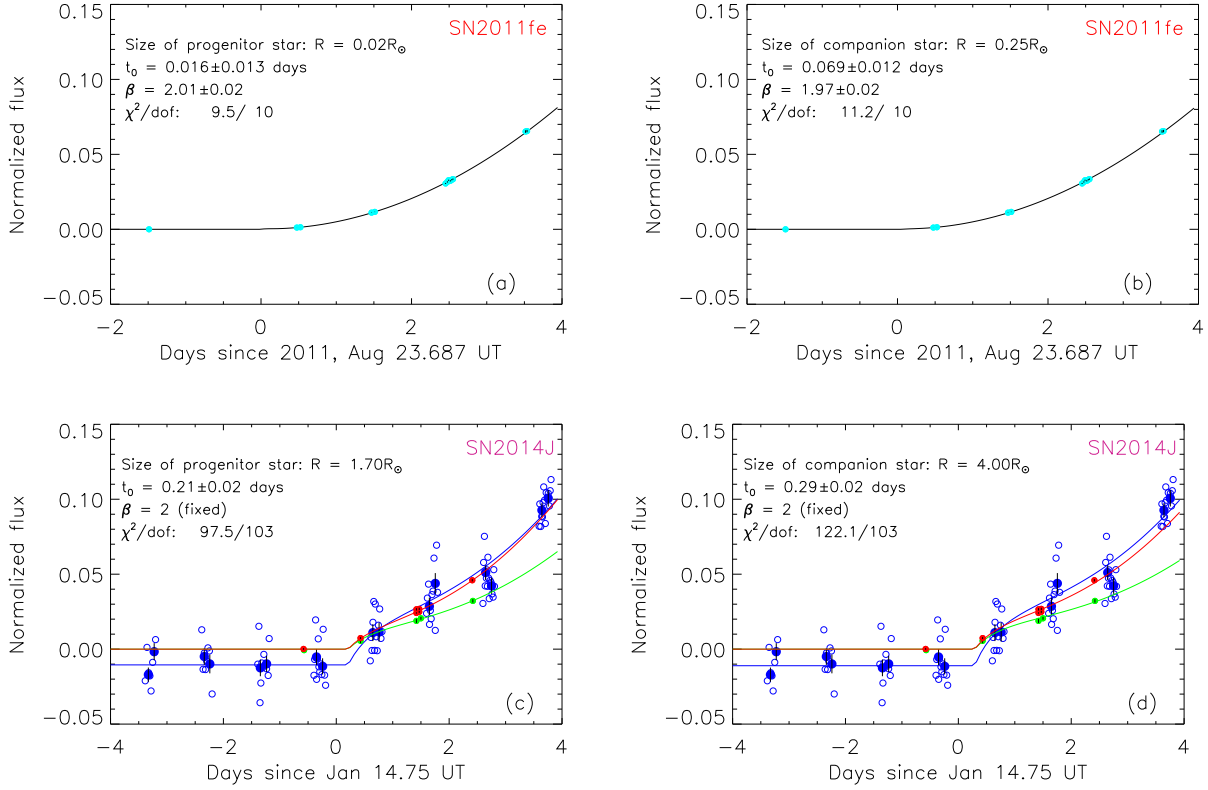


Fig. 2.— Fits of early g -band lightcurve points and limits of SN 2011fe from Nugent et al. (2011) (above) and the broad-band KELT observations (Siverd et al. 2014) and the two narrow-band H_α photometry of SN 2014J from Goobar et al. (2014) (below). Open symbols show individual KELT photometry points, while the blue filled symbols show the data combined into two bins for each night. Blue lines show the fitted model. Red and green bullets show the iPTF data for the two narrow-band filters shown in Fig. 1. Similarly, the fitted models to those data points are shown in same color. Panels (a) and (c) show the fits where the lightcurves are assumed to have a contribution from the heated progenitor ejecta. Panels (b) and (d) investigate the possibility of heating of a companion star, following Kasen (2010). A small residual host galaxy contamination in the KELT photometry is fitted as a free (constant) parameter.

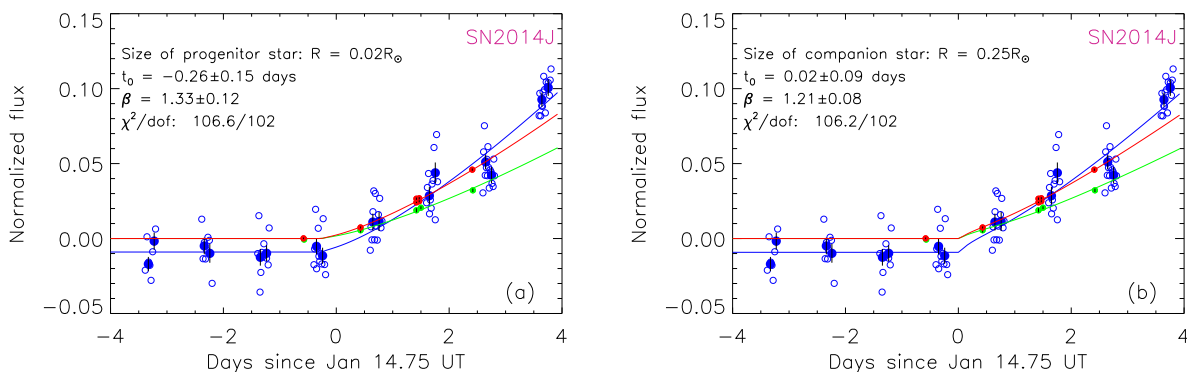


Fig. 3.— Lightcurve fits of SN 2014J fixing the size of the progenitor to be the same as for SN 2011fe (a), and invoking the same size for an allowed companion star as for SN 2011fe (b). Instead, the power-law parameter, β , is allowed to vary freely. Open symbols show individual KELT photometry points, while the blue filled symbols show the data combined into two bins for each night. Blue lines show the fitted model. Red and green bullets show the iPTF data for the two narrow-band filters shown in Fig. 1. Similarly, the fitted models to those data points are shown in same color. Good fits are found, although for significantly flatter rise time, $\beta \sim 1.2 - 1.3$.

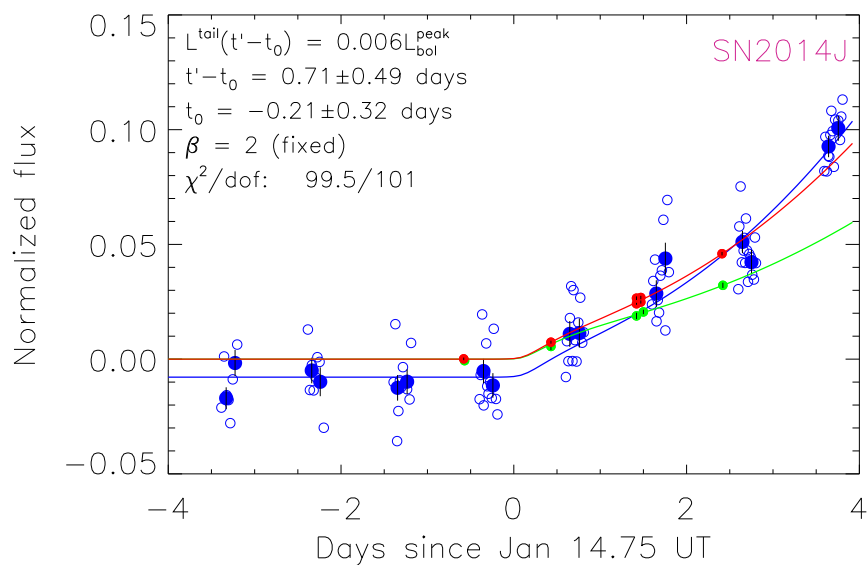


Fig. 4.— Lightcurve fits of SN 2014J assuming early rise has contributions from surface radioactivity Piro & Nakar (2013), as described in Section 4.4. Open symbols show individual KELT photometry points, while the blue filled symbols show the data combined into two bins for each night. Blue lines show the fitted model. Red and green bullets show the iPTF data for the two narrow-band filters shown in Fig. 1. Similarly, the fitted models to those data points are shown in same color.